

Neutrino Clustering in Cold Dark Matter Halos : Implications for Ultra High Energy Cosmic Rays

Shwetabh Singh* and Chung-Pei Ma†

*Department of Astronomy,
University of California at Berkeley,
601 Campbell Hall, Berkeley, CA 94720*

We develop a method based on the collisionless Boltzmann equation to calculate the gravitational clustering of relic neutrinos in realistic cosmological models dominated by cold dark matter (CDM) and the cosmological constant. This method can be used to estimate the phase-space distribution of any light particles in CDM halos. We find that neutrinos with masses $\gtrsim 0.3$ eV cluster appreciably in dark matter halos above the galactic size. The resulting neutrino overdensity above the cosmic mean neutrino density increases with both the neutrino mass and the halo mass, ranging from ~ 10 for 0.3 eV neutrinos in $\sim 10^{13} M_\odot$ halos to ~ 1500 for 1.8 eV neutrinos in $\sim 10^{15} M_\odot$ halos. We examine the implications of neutrino clustering for the Z-burst model of ultra high energy cosmic rays (UHECR), which interprets the observed events at $E > 4 \times 10^{19}$ eV as decay products of Z-bosons from the resonant scattering between relic and high energy neutrinos and anti-neutrinos. We estimate the UHECR energy spectrum for various neutrino masses towards five of the most massive clusters in the local universe (within 100 Mpc): Virgo, Perseus-Pisces, Hydra, Centaurus, and Coma. The UHECR flux in the Z-burst model is expected to be significantly higher towards these clusters if $m_\nu \gtrsim 0.3$ eV and nearly isotropic otherwise.

I. INTRODUCTION

The nature of cosmic rays above the Greisen-Zatsepin-Kuzmin (GZK) cutoff [1] at $\sim 4 \times 10^{19}$ eV is an unsolved problem in ultra high energy cosmic ray (UHECR) physics [2]. These events have been reported by the Akemo Giant Air Shower Array (AGASA) [3], Fly's Eye [4], Haveria Park [5], HiRes [6], and Yakutsk [7] collaborations. Interactions with the cosmic background photons γ_{cmb} via photoproduction of pions ($p\gamma_{cmb} \rightarrow p + N\pi$, $n\gamma_{cmb} \rightarrow n + N\pi$), photopair production ($p\gamma_{cmb} \rightarrow pe^+e^-$, $\gamma\gamma_{cmb} \rightarrow e^+e^-$), and inverse Compton scattering ($e^\pm\gamma_{cmb} \rightarrow e^\pm\gamma$, $p\gamma_{cmb} \rightarrow p\gamma$) at high energies [8] constrain a $\sim 10^{20}$ eV cosmic ray to a few Mpc for the characteristic lengths of either charged cosmic rays or neutrons and photons. More specifically, the attenuation length of protons above the GZK cutoff is ~ 50 Mpc. The lack of known processes to accelerate cosmic rays in small Galactic objects makes the Galactic origin of these ultra high energy particles unfeasible [9]. Novel powerful acceleration mechanisms for light nuclei are required if these energetic particles are produced in nearby galaxies [10]. Exotic particles and dynamics have also been suggested, but these come with their own difficulties [2].

One proposed explanation for the UHECRs is the Z-burst model, which tries to solve the puzzle without invoking new physics beyond the standard model of particle physics except for neutrino masses. Several recent experiments [11–14] have found evidence for non-zero neutrino mass. The Z-burst model hinges on the fact that ul-

tra high energy neutrinos (and anti-neutrinos) produced at cosmological distances can reach the GZK zone unattenuated. Their resonant annihilation on the relic anti-neutrinos (and neutrinos) produces Z bosons, about 70% of which decay into hadrons within $\sim 10^{-25}$ sec. The final state has fifteen pions and 1.35 baryon-antibaryon pairs on average [15], where the fifteen pions decay into thirty high energy photons. The Z boson is highly boosted ($\sim 10^{10}$) [16], resulting in a highly collimated beam with a half angle of $\sim 10^{-10}$. This and the fact that the effect of magnetic fields at such high energies is negligible [17] ensure a high probability for the protons and photons to reach the observer if the Z-burst occurs in the direction of the Earth. The Z-burst model has been discussed in detail in many papers [18–24]. The resulting cosmic ray flux has been shown to depend strongly on the density of the relic neutrinos [15, 16, 20, 25, 26], but the neutrino density in these calculations has been taken to be either the constant relic density from the big bang or some ad hoc value.

In this paper we perform a detailed calculation of the neutrino clustering in the local universe using realistic cosmological models and apply the results to the Z-burst model for UHECRs. Since the current constraints from cosmological observations and laboratory experiments indicate that the neutrino masses are small ($\lesssim 2$ eV; see Sec II) and the CDM dominates the dark matter density ($\Omega_{cdm} \gg \Omega_\nu$), we do not expect the clustering of neutrinos to affect significantly that of the CDM. As a result, it is not essential to use full scale, time consuming N -body simulations. Instead, we solve the collisionless Boltzmann equation for the neutrino phase space distribution in a background potential given by the universal profile of CDM halos reported in recent high resolution simulations [27]. The Boltzmann equation is then linear

*shwetabh@astro.berkeley.edu

†cpma@astro.berkeley.edu

in the neutrino density contrast and has tractable integral solutions. The advantage of this method over the conventional N -body simulations is that we can obtain the neutrino density profile much below the resolution scale (~ 50 kpc) of large cosmological simulations by using as an input the CDM potential determined from much higher resolution simulations of individual halos. Moreover, the computation time required for our approach is negligible compared with numerical simulations, thereby allowing us to explore a large parameter space of neutrino masses and dark matter halo masses.

In Sec II the relevant Boltzmann equation and the integral solutions are derived. In Sec III results for the clustering of neutrinos for different neutrino masses and CDM halos are presented and compared with physical arguments based on neutrino free streaming and the Tremaine-Gunn constraint [28]. The resulting neutrino density profiles are also compared with earlier N -body simulations [29], which show good agreement. In Sec IV the neutrino overdensity calculation is incorporated in the Z-burst model for UHECRs, where we make realistic predictions for the UHECR energy spectrum for different neutrino masses. We estimate the level of anisotropy in the UHECR flux by examining lines of sight towards five of the most massive clusters (Virgo, Perseus-Pisces, Hydra, Centaurus, and Coma) in the local universe (within 100 Mpc) where neutrinos are likely to be most clustered.

II. BOLTZMANN EQUATION FOR NEUTRINO CLUSTERING IN CDM HALOS

In this section we develop an approach based on the collisionless Boltzmann equation to study how massive neutrinos cluster gravitationally in realistic cosmological models. We start by noting that the median velocity of unclustered background neutrinos of mass m_ν (in eV) at redshift z is

$$\bar{v} = 161(1+z)m_\nu^{-1} \text{ km s}^{-1}. \quad (1)$$

This implies that light neutrinos ($m_\nu \lesssim 2$ eV) do not accrete significantly onto CDM protoclusters until $z \sim 3$ because the neutrino thermal velocities are greater than the velocity dispersion of a typical cluster or supercluster. We are then faced with the more tractable problem of how neutrinos cluster in the potential well of an existing CDM halo. Our approach is to use the collisionless Boltzmann equation for the neutrino phase space density f and follow its evolution in a background CDM potential given by the approximate universal profile obtained in high resolution simulations of individual halos [27]. Note that the CDM potential is time-dependent in general. Earlier work has used the Boltzmann approach to study how neutrinos cluster around point masses in the context of cosmic string seeded galaxy formation [30, 31]. This method allows us to calculate the neutrino density profiles in the inner part of the cluster ($\lesssim 10$ kpc) that can not be resolved by large cosmological simulations.

This will be seen to be important in the Z-burst model where a significant contribution to the cosmic ray flux comes from the inner regions of the halo.

In the Newtonian approximation and in physical coordinates, the collisionless Boltzmann equation takes the form

$$\frac{\partial f}{\partial t} + \dot{\mathbf{r}} \cdot \nabla_{\mathbf{r}} f + \dot{\mathbf{p}} \cdot \nabla_{\mathbf{p}} f = 0. \quad (2)$$

Rewriting it in conformal time $d\tau = dt/a$ and in comoving position $\mathbf{x} = \mathbf{r}/a$ and momentum $\mathbf{q} = a\mathbf{p} - m_\nu \dot{a}\mathbf{r}$, we obtain

$$\begin{aligned} \frac{1}{a} \frac{\partial f}{\partial \tau} + \frac{\mathbf{q}}{m_\nu a^2} \cdot \nabla_{\mathbf{x}} f - m_\nu \ddot{a} \mathbf{x} \cdot \nabla_{\mathbf{q}} f \\ - m_\nu \nabla_{\mathbf{x}} \Phi \cdot \nabla_{\mathbf{q}} f = 0, \end{aligned} \quad (3)$$

where the Newtonian gravitational potential Φ obeys $\dot{\mathbf{p}} = -m_\nu \nabla \Phi$. At the time of decoupling the neutrino phase space density is given by the thermal Fermi-Dirac distribution $f_0(q) \propto (e^{q/T_{\nu,0}} + 1)^{-1}$ where $T_{\nu,0} = (4/11)^{1/3} T_{\gamma,0} = 1.676 \times 10^{-4}$ eV is the temperature of the neutrino background today. Gravitational clustering distorts the spatially uniform f_0 , so we write the full distribution as

$$f(\mathbf{x}, \mathbf{q}, \tau) = f_0(q) + f_1(\mathbf{x}, \mathbf{q}, \tau). \quad (4)$$

The gravitational potential can also be written as

$$\Phi(\mathbf{x}, \tau) = \Phi_0(\mathbf{x}, \tau) + \Phi_1(\mathbf{x}, \tau), \quad (5)$$

where Φ_0 is related to the mean background comoving density $\bar{\rho} = \bar{\rho}_{\text{cdm}} + \bar{\rho}_\nu$ by $\nabla_{\mathbf{x}} \Phi_0 = \frac{4\pi}{3} G \bar{\rho} a^2 \mathbf{x}$, and Φ_1 is determined by the density contrast of both CDM and neutrinos in the halo:

$$\nabla_{\mathbf{x}}^2 \Phi_1 = 4\pi G a^2 (\delta\rho_{\text{cdm}} + \delta\rho_\nu) \quad (6)$$

Eq. (3) then becomes

$$\begin{aligned} \frac{1}{a} \frac{\partial f_1}{\partial \tau} + \frac{\mathbf{q}}{m_\nu a^2} \cdot \nabla_{\mathbf{x}} f_1 - m_\nu \nabla_{\mathbf{x}} \Phi_1 \cdot \nabla_{\mathbf{q}} f_0 \\ - m_\nu \nabla_{\mathbf{x}} \Phi_1 \cdot \nabla_{\mathbf{q}} f_1 = 0, \end{aligned} \quad (7)$$

where we have used the Friedmann equation $\ddot{a} = -\frac{4\pi}{3} G \bar{\rho} a$, which gives $\ddot{a} \mathbf{x} + \nabla_{\mathbf{x}} \Phi_0 = 0$. We note that eq. (7) is the full Boltzmann equation and no approximation has been made thus far. It is generally a nonlinear equation in f_1 where Φ_1 is related to f_1 . For our problem, however, Φ_1 is mostly determined by the CDM whose potential has a well known, pre-determined form. Eq. (7) is then linear in f_1 and much easier to solve.

Furthermore, eq. (7) has a simple integral solution if the fourth term is neglected. For example, in earlier calculations that examined neutrino clustering onto point masses seeded by cosmic strings, this term was dropped in order to simplify the calculation [30, 31]. We will also drop this term, but we justify this approach in two ways. First, we note that dropping this term requires

$\nabla_q f_1 < \nabla_q f_0$ and not $f_1 < f_0$. The former is generally a less restrictive condition and can be satisfied even if f_1 is much larger than f_0 because on dimensional grounds, we have

$$\frac{\nabla_q f_1}{\nabla_q f_0} \sim \frac{f_1/\sigma_v}{f_0/\bar{v}} \sim \frac{\delta\rho_\nu/\sigma_v^4}{\bar{\rho}_\nu/\bar{v}^4} \sim \delta_\nu \left(\frac{\bar{v}}{\sigma_v} \right)^4, \quad (8)$$

where σ_v is the velocity dispersion of the gravitational potential Φ_1 and \bar{v} is the median neutrino thermal velocity in eq. (1). Since only neutrinos with $\bar{v} \ll \sigma_v$ are cold enough to fall into the gravitational wells, we expect the ratio $\nabla_q f_1/\nabla_q f_0$ to be much smaller than f_1/f_0 , thereby making it easier to justify the dropping of the fourth term in eq. (7). (For example, $\nabla_q f_1/\nabla_q f_0 \lesssim 0.2$ for ~ 1 eV neutrinos in $\sim 10^{14} M_\odot$ halos.) Eq. (8) further indicates that the neutrino overdensity is larger than f_1/f_0 by $(\sigma_v/\bar{v})^3$, a large factor in highly clustered regions. This explains qualitatively the large overdensity found in our numerical results to be presented in Sec III. In the next section we also provide further justification for ignoring the $\nabla_q f_1$ term by comparing our results with the neutrino density profiles of two halos obtained from earlier numerical simulations.

Following [30], we convert eq. (7) into an ordinary differential equation by going into Fourier space and using a new time variable $d\eta = d\tau/a$:

$$\frac{\partial \tilde{f}_1}{\partial \eta} + \frac{i\mathbf{k} \cdot \mathbf{q}}{m_\nu} \tilde{f}_1 + \frac{im_\nu}{k^2} 4\pi G a^4 \tilde{\rho} \mathbf{k} \cdot \nabla_q f_0 = 0, \quad (9)$$

where \tilde{f}_1 and $\tilde{\rho}$ are the Fourier transforms of f_1 and ρ . The solution is

$$\begin{aligned} \tilde{f}_1(\mathbf{k}, \mathbf{q}, \eta) = & -\frac{im_\nu}{k^2} 4\pi G \int_{\eta_0}^{\eta} d\eta' e^{-i\mathbf{k} \cdot \mathbf{q}(\eta-\eta')/m_\nu} \\ & \times a^4(\eta') \tilde{\rho}(\mathbf{k}, \eta') \mathbf{k} \cdot \nabla_q f_0, \end{aligned} \quad (10)$$

where we have taken the initial neutrino phase space to be homogeneous, i.e., $f_1(\eta_0) = 0$ and $f(\eta_0) = f_0$.

The comoving neutrino number density is given by

$$\tilde{n}_\nu(\mathbf{k}, \eta) - \bar{n}_\nu = \frac{2}{h_p^3} \int d^3 q \tilde{f}_1(\mathbf{k}, \mathbf{q}, \eta), \quad (11)$$

which can be obtained from eq. (10) after integration by parts in q and integration over angles:

$$\begin{aligned} \tilde{n}_\nu(\mathbf{k}, \eta) - \bar{n}_\nu = & \frac{32\pi^2 G m_\nu}{h_p^3 k} \int_{\eta_0}^{\eta} d\eta' a^4(\eta') \tilde{\rho}(k, \eta') \\ & \times \int_0^\infty dq q \frac{\sin[k q (\eta - \eta')/m_\nu]}{e^{q/T_{\nu,0}} + 1} \end{aligned} \quad (12)$$

where $\bar{n}_\nu \approx 112 \text{ cm}^{-3}$ is the cosmic mean comoving number density of one species of light neutrinos and antineutrinos, and h_p is the Planck constant. Eq. (12) is the main equation that we will solve in this paper. It is a Volterra integral equation of the second kind that has the form $f(t) = \int_a^t ds K(t, s)f(s) + g(t)$ and can be solved

with the trapezoidal rule. It describes how neutrinos of a given mass m_ν cluster around a realistic CDM halo as a function of time. The density of the halo at a given time, $\bar{\rho}$, should generally be the sum of the CDM and the neutrino components, but as we verify below, using the CDM potential alone is a very good approximation for the cosmological models of current interest.

III. RESULTS FOR NEUTRINO CLUSTERING IN CDM HALOS

In this section we present results for n_ν computed from eq. (12). We choose to integrate eq. (12) from $z = 3$ to 0; the results differ by only about 5% if the initial redshift is pushed back to 5 because the neutrinos do not cluster appreciably at such early times as discussed above. We also need to specify the cosmological models and neutrino masses. For the cosmological parameters, we use the currently favored critically-flat model with matter density $\Omega_m = \Omega_{\text{cdm}} + \Omega_\nu = 0.35$, cosmological constant $\Omega_\Lambda = 0.65$, and Hubble parameter $h = 0.7$. Variations in these parameters at 10 to 20% level are not expected to alter our neutrino results significantly since the effect on the halo potential Φ_1 is small. For the neutrino masses, we consider four different models in which three models assume three degenerate massive species with masses 0.6, 0.3, and 0.15 eV respectively, and one model with one massive species with mass 1.8 eV. The corresponding density parameter in neutrinos is $\Omega_\nu \approx 0.04, 0.02, 0.01$ and 0.04, respectively, all much smaller than Ω_{cdm} . This range of neutrino masses is chosen to span the current cosmological and laboratory limits. The most recent cosmological constraint comes from the galaxy clustering power spectrum of 2-Degree-Field Redshift Survey, which places an upper limit of 1.8 eV on the sum of the neutrino masses [32]. The Super-Kamiokande experiment [11] provides strong evidence for oscillations between neutrino species with a mass difference of $\delta m^2 = (1 - 8) \times 10^{-3}$ eV, giving a minimum mass of ≈ 0.07 eV if the neutrino masses are hierarchical. The choice of three degenerate neutrino masses is based on indications that if any of the mass eigenvalues is above 0.1 eV then all three masses are above 0.1 eV and almost degenerate [33].

Although the final neutrino density profile will depend strongly on the CDM profile, we do not expect the reverse to hold: CDM density will not be much affected by the clustering of neutrinos because all the models considered in this paper have small $\Omega_\nu/\Omega_{\text{cdm}}$, so the CDM dominates the gravitational potential of a dark matter halo. We are therefore justified in using the universal CDM profile determined from the high resolution pure CDM simulations [27] as the input:

$$\rho_{\text{cdm}}(r) = \frac{\bar{\rho} \bar{\delta} r_s^3}{r(r+r_s)^2}, \quad (13)$$

where $\bar{\delta}$ and r_s are given in terms of the concentration

parameter [34, 35]

$$\begin{aligned} c &= \frac{9}{1+z} \left(\frac{M}{1.5 \times 10^{13} h^{-1} M_\odot} \right)^{-0.13}, \\ \bar{\delta} &= \frac{200c^3}{3[\ln(1+c) - c/(1+c)]}, \\ r_s &= \frac{1.63 \times 10^{-5}}{\Omega_m^{1/3} c} \left(\frac{M}{h^{-1} M_\odot} \right)^{1/3} h^{-1} \text{Mpc}. \end{aligned} \quad (14)$$

We evaluate the mass density ρ on the right hand side of eq. (12) exactly by adding the CDM density given above and the neutrino density computed from previous time steps. We did find that approximating ρ with the CDM profile alone (i.e. ignoring the neutrino contribution to the total potential) changes our results by no more than 10% for the light neutrino masses and cosmological parameters considered in this paper. We also tested the simplifying assumption made in [30], which allowed them to reduce the integrals in eq. (12) analytically to a single integral by using $(e^{q/T_{\nu,0}} + 1)^{-1} = A e^{-q/T_{\nu,0}}$, i.e., by assuming a Maxwell-Boltzmann instead of Fermi-Dirac distribution. We found this simplification to cause a $\sim 20\%$ difference at small scales, so we do not use this approximation here.

Before presenting our results for the realistic models above, we first conduct a comparison study by checking our results for the neutrino density profile against those in the numerical simulations of Ref. [29], which investigated the clustering of CDM and neutrinos in two flat cosmological models: $\Omega_{\text{cdm}} = 0.8$ and $\Omega_\nu = 0.2$ with two species of 2.3 eV neutrinos, and $\Omega_{\text{cdm}} = 0.7$ and $\Omega_\nu = 0.3$ with one species of 7 eV neutrinos. Both models assumed $h = 0.5$. These models are no longer consistent with current observations, but the simulation results provide a useful tool for us to test the validity of our Boltzmann approach. For a fair comparison, we use the CDM halo profile found in [29] as an input:

$$\rho_{\text{cdm}}(r) = \frac{C}{r(r+R)^\alpha}, \quad (15)$$

where R and α are 0.3 Mpc and 1.5 for the $\Omega_\nu = 0.2$ model and 0.11 Mpc and 1.1 for the $\Omega_\nu = 0.3$ model. We note that their outer profile is shallower than eq. (13) from the pure CDM simulations [27]. In Ref. [29] this difference was attributed to the differing spectral index n for the matter power spectrum of the neutrino models at the mass scale of the simulated halos ($\approx 1.3 \times 10^{15} M_\odot$): $n \simeq -1.36$ for $\Omega_\nu=0.2$ and $n \simeq -1.53$ for $\Omega_\nu=0.3$. This argument, however, appears inconsistent with the near universal nature of the halo density profile reported in Ref. [27]. A better understanding for the origin of halo profiles should help resolve this issue.

Fig. 1 compares the ratio of the neutrino and CDM density profiles from our approach vs. the two simulated halos in Ref. [29]. For both halos we have used the same cosmological parameters, CDM profiles, and halo mass in our Boltzmann approach as in their simulations. We

find a good agreement between the two methods for the outer parts of the cluster; whereas our results are lower by about 50% in the inner parts. This discrepancy may be due to our neglecting the fourth term in eq. (7), or due to statistical fluctuations in the substructure in their simulations. (Only two simulated halos are presented in Ref. [29].) The Boltzmann approach used here also allows us to explore how neutrinos respond to different CDM potentials. As an illustration of this, we show in Fig. 1 how the neutrino profile changes when the input CDM profile is changed from eq. (15) to the higher resolution profile of eq. (13). We conclude from Fig. 1 that we can obtain a reasonable estimate for neutrino clustering using eq. (12) instead of full scale N -body simulations.

We now turn to our results for the realistic cosmological models and neutrino masses given at the beginning of this section. The four panels in Fig. 2 show the neutrino overdensity n_ν/\bar{n}_ν computed from eq. (12) for four models of neutrino masses. The more massive neutrinos clearly cluster more because of their lower thermal velocities. Within each panel, the four curves illustrate how n_ν increases with halo masses from 10^{12} to $10^{15} M_\odot$ as a result of the deeper halo gravitational potentials. The growth of n_ν in the inner parts of the halo, where it is almost independent of r , is illustrated in Fig. 3 for 0.7 and 0.4 eV neutrinos in 10^{15} , 10^{14} , and $10^{13} M_\odot$ halos. Most of the clustering is seen to occur at low redshifts.

Unlike the CDM density that continues to rise towards the inner part of a halo as $\rho \propto 1/r$, all curves in Fig. 2 show that n_ν flattens out at some radius. Similar features were also seen in Ref. [31] for neutrinos clustered around cosmic strings. This relative suppression in the neutrino vs. CDM overdensity reflects neutrino free streaming, which dampens and retards perturbation growth on small length scales due to phase mixing. The neutrino damping scale, R_d , can be characterized by the length scale above which neutrinos behave like the CDM. The standard method to solve the Boltzmann equation for a fluid with pressure involves the transformation of the Boltzmann equation into an infinite hierarchy of velocity moment equations [36], where the lowest three moments with $l = 0, 1$, and 2 correspond to the density, velocity, and shear of the fluid. The choice of the truncation of the hierarchy depends on the physical properties of the fluid and the length scales. For CDM, for example, all modes above $l = 1$ are zero. The parameter R_d gives the scale above which the Boltzmann hierarchy for neutrinos can be truncated at $l = 1$ (as for the CDM), and below which more l -modes must be included to compute the neutrino damping effect accurately. This scale is given by [37]

$$R_d(\tau) \equiv \frac{\tau}{\sqrt{1 + [a(\tau)/a_{nr}]^2}}, \quad (16)$$

where $a_{nr} \simeq 3T_{\nu,0}/m_\nu$ is the expansion factor at which the neutrinos become non-relativistic. For the cosmological models considered in this paper, the scale is $R_d(z=0) \approx 5.8/m_\nu(\text{eV})$ Mpc. From Fig. 1, we indeed find the ratio $\rho_\nu/\rho_{\text{cdm}}$ to be about the cosmic mean

value Ω_ν/Ω_{cdm} at scales above R_d and to decrease gradually at smaller radii (top panels), with a final flattening in the neutrino overdensity at $r \sim 0.1 R_d$ (bottom panels). Fig. 2 shows that the radius at which δ_ν flattens out depends weakly on the mass of the CDM halo. It occurs at smaller radii for less massive CDM halos primarily because the lower mass halos provide shallower potential wells. The damping scale R_d of eq. (16) is to be contrasted with the neutrino free streaming distance, which is typically defined as the comoving distance traversed from the time of neutrino decoupling to a_{nr} : $\lambda_{fs} \equiv \int_{\tau_i}^{\tau_{nr}} d\tau'/a(\tau') \simeq 600/m_\nu(\text{eV}) \text{ Mpc}$ [38]. The distance λ_{fs} reflects the global streaming motion of neutrinos but not the local clustering properties of neutrinos around CDM after they become non-relativistic.

Another way to understand the results in Figures 1 and 2 is to compare the thermal velocities of neutrinos with the velocity dispersions of the CDM halos: neutrinos can cluster significantly only if their mean thermal velocity in eq. (1) is below the typical velocity of the host CDM halo. Fig. 4 compares these two characteristic velocities for a range of neutrino masses and halo masses. Since the NFW profile specifies only the spatial and not the velocity distribution of the CDM halo particles, two velocity ellipsoids are shown for comparison: isotropic, which is appropriate near the center of the halo, and the more radial distribution $\beta = 1 - v_t^2/v_r^2 = 0.5$, which is appropriate for the outer regions. Fig. 4 illustrates that $< 0.15 \text{ eV}$ neutrinos are too hot to be captured significantly by $\lesssim 10^{14} M_\odot$ halos, while the more massive neutrinos can fall into progressively lower mass halos, a result consistent with that shown in Fig. 2.

Our results for neutrino clustering can be compared with the Tremaine-Gunn bound [28], which gives an upper limit on the neutrino density in the core of a halo based on the argument that the maximum coarse grained phase space density can not exceed the maximum initial phase space density due to phase mixing. Their results are not directly applicable to our problem because in their derivation, neutrinos are assumed as the sole constituent of dark matter, and the coarse grained neutrino distribution is assumed to be Maxwell-Boltzmann instead of Fermi-Dirac for computational convenience. More recent work [39] has extended the derivation to models including both CDM and neutrinos and obtained $\rho_\nu \leq |2\Phi|^{3/2} m_\nu^4 / 12\pi^4$, where Φ is the gravitational potential of the system. For the NFW profile, we find

$$\frac{n_\nu}{\bar{n}_\nu}(r; m_\nu, r_s, \bar{\delta}) \lesssim 40 \left(\frac{m_\nu}{\text{eV}}\right)^3 \left(\frac{r_s}{\text{Mpc}}\right)^3 \bar{\delta}^{3/2}$$

$$\times \left[\frac{r_s}{r} \ln \left(\frac{r}{r_s} + 1 \right) \right]^{3/2}, \quad (17)$$

where r_s and $\bar{\delta}$ are the CDM halo parameters given by eq. (14). For 1.8 eV neutrinos, for example, this formula gives $n_\nu/\bar{n}_\nu < 3.9 \times 10^4, 3.2 \times 10^5, 2.7 \times 10^6$, and 2.3×10^7 for $10^{12}, 10^{13}, 10^{14}$ and $10^{15} M_\odot$ halos, respectively, at the scale radius r_s . One can see that this constraint is satisfied by at least three orders of magnitude for all neutrino overdensities in Figures 1 and 2.

IV. IMPLICATIONS FOR ULTRA HIGH ENERGY COSMIC RAYS

In this section we apply the neutrino clustering results from Sec III to the Z-burst model for UHECRs. No previous work on the Z-burst model has included realistic calculations for n_ν . Instead, the value of n_ν has been chosen based on certain observational constraints [24] or physical arguments [16, 20] and has differed greatly from $n_\nu \sim (1 - 10^5)\bar{n}_\nu$. For instance, in [24], it is inferred from the CDM distribution in our local universe, but the large smoothing scale $\sim 20 \text{ Mpc}$ assumed in the calculation results in $n_\nu \sim \bar{n}_\nu$. In contrast, our results from Sec III show that n_ν can be $\gg \bar{n}_\nu$ in the inner $\sim 1 \text{ Mpc}$ of CDM halos. In Refs. [16, 20], n_ν is approximated based on phase-space arguments similar to that of [28]. While this approach gives an upper bound on the neutrino clustering, the actual overdensity can be significantly less, as we have discussed in the previous paragraph. In addition, the neutrino clustering scale of $\approx 5 \text{ Mpc}$ assumed in [20] is much larger than what we find in our calculations. Our method gives specific predictions for n_ν as a function of halo radius, halo mass, and neutrino mass.

To estimate the cosmic ray flux we follow the standard assumption in the Z-burst model that the UHECRs above the GZK cutoff are produced by the resonant $\nu\bar{\nu}$ scattering, while the lower energy events are explained by protons originating from a uniform distribution of extragalactic sources. The latter appears consistent with the isotropic distribution of $E < 4 \times 10^{19} \text{ eV}$ events detected in AGASA and HiRes [40]. We compute the cosmic ray flux (in $(\text{eV m}^2 \text{ s sr})^{-1}$) from the Z-burst model with [24]

$$F_Z(E) = \int_0^\infty dE_p \int_0^{R_{max}} dr \left[\int_0^\infty dE_{\nu_i} F_{\nu_i}(E_{\nu_i}, r) n_{\bar{\nu}_i}(r) + \int_0^\infty dE_{\bar{\nu}_i} F_{\bar{\nu}_i}(E_{\bar{\nu}_i}, r) n_{\nu_i}(r) \right] \times \sigma_{\nu\bar{\nu}}(s) \text{Br}(Z \rightarrow \text{hadrons}) \frac{dN_{p+n}}{dE_p} \left| \frac{\partial P_p(r, E_p; E)}{\partial E} \right|. \quad (18)$$

Here $F_{\nu_i}(E_{\nu_i}, r)$ is the flux of ultra high energy neutrinos with energy E_{ν_i} at distance r and $n_{\nu_i}(r)$ is the physical number density of the relic neutrinos. (The repeated index i is summed over different neutrino species.) The particle interactions are described by the cross section $\sigma_{\nu\bar{\nu}}(s)$ for the Z-boson production at the center-of-mass energy $s = 2m_\nu E_\nu$, and by the branching ratio $\text{Br}(Z \rightarrow \text{hadrons}) = 69.89 \pm 0.07\%$ for the subsequent cascade of the Z-boson into hadrons [41]. The factor dN_{p+n}/dE_p gives the energy distribution of the produced protons and neutrons. The subsequent proton propagation is specified by $P_p(r, E_p; E)$, which gives the probability that a proton created at distance r with energy E_p arrives at Earth with an energy greater than E . It measures the amount of proton energy degradation due to the resonant photoproduction of pions and other processes discussed in Sec I. Specific values of P_p has been calculated in [42] for the range of parameters considered in this paper. We do not include in our UHECR flux estimate the contributions from the photons produced in the Z-decay because experimental data suggest that less than 50% of the cosmic rays above 4×10^{19} eV are photons at the 95% confidence level [43, 44]. Typical physical mechanisms used to explain the suppressed photon contributions are large universal radio background and sufficiently strong extragalactic magnetic fields ($\gtrsim 10^{-9}$ Gauss) [24, 45]. The study of the effects of these parameters on the UHECR flux due to the Z-burst model can be a subject of future work.

A key feature of the Z-burst model is that the cross section $\sigma_{\nu\bar{\nu}}(s)$ for $\nu\bar{\nu} \rightarrow Z^0$ is enhanced by several orders of magnitude near the resonant energy in the rest frame of the relic neutrinos [18]

$$E_{\nu_i}^{res} = \frac{M_Z^2}{2m_{\nu_i}} = 4.2 \times 10^{21} \text{eV} \left(\frac{1 \text{eV}}{m_{\nu_i}} \right), \quad (19)$$

where M_Z is the mass of the Z boson. The flux in eq. (18) to a good approximation therefore depends only on the neutrino resonant energy and not on the slope of the incident high energy neutrino spectrum. Eq. (18) can then be written as [24]

$$F_Z(E) = \bar{\sigma}_{\nu\bar{\nu}} F_{\nu_i}(E_{\nu_i}^{res}) \int_0^\infty dE_p \int_0^{R_{max}} dr \\ \times n_{\nu_i}(r) Q_p \left(y = \frac{4m_\nu E_p}{M_Z^2} \right) \\ \times \left| \frac{\partial P_p(r, E_p; E)}{\partial E} \right|, \quad (20)$$

where $n_{\nu_i}(r)$ is the physical number density of neutrinos and antineutrinos at the Z-burst site at radial distance r , $\bar{\sigma}_{\nu\bar{\nu}} = 40.4$ nb is the cross section for $\nu\bar{\nu} \rightarrow Z^0$ averaged over the width of the resonance, and $F_{\nu_i}(E_{\nu_i}^{res})$ is the incident flux of ultra high energy neutrinos at the resonant energy. The function Q_p is the boosted momentum distribution from hadronic Z decays and can be calculated from experimental data [24]. It has a fairly broad peak at

$y \approx 10^{-2}$ and falls off approximately as y^{-7} for $y \gtrsim 0.5$. The neutrino flux $F_{\nu_i}(E_{\nu_i}^{res})$ remains a free parameter in the Z-burst calculation since no successful astrophysical model yet exists to explain the production of $\gtrsim 10^{21}$ eV neutrinos [46–48]. We do not attempt to model the effect of source evolution in our calculations since it is again an unknown quantity and is easy to incorporate once its nature is known.

We first present results for the cosmic ray spectrum $F(E)$ in the Z-burst model ignoring the spatial clustering in the neutrinos, i.e., we assume $n_\nu = \bar{n}_\nu$ in eq. (20). This assumption underestimates the flux in the Z-burst model, but we include the results here for comparison since this is a common assumption made in several Z-burst calculations [16, 24, 48]. Fig. 5 shows the sensitivity of $E^3 F(E)$ on the neutrino masses. The flux is higher at high energies for smaller m_ν because the momentum distribution Q_p of the decay particles peaks at a higher energy for smaller m_ν . For a given m_ν , $E^3 F(E)$ decreases rapidly at $E \gtrsim 10^{21}$ eV because Q_p falls off as $\sim y^{-7}$ for $y \gtrsim 0.5$. The integration is carried out to a maximum distance of $R_{max} = 2000$ Mpc, but our results are insensitive to this choice as long as R_{max} is sufficiently beyond the GZK zone of ~ 50 Mpc.

For ease of comparison, the curves in Fig. 5 are all normalized to the same incident neutrino flux of $F_{\nu_i}(E_{\nu_i}^{res}) = 1.7 \times 10^{-35} (\text{eV m}^2 \text{s sr})^{-1}$ for each of the three neutrino flavors. (For the one flavor 0.07 eV model, the assumed flux is 3 times higher.) We do not attempt to determine this value by performing statistical fits to data because the UHECR spectrum from AGASA (square symbols) and HiRes (triangle symbols) disagree in both amplitude and shape. We do note that for models that have three degenerate neutrino masses of $m_{\nu_i} \lesssim 1$ eV, this value for the neutrino flux is consistent with the existing upper bound from the Goldstone Lunar Ultra-high energy neutrino Experiment (GLUE) [49]. The 0.07 eV model shown in Fig. 5, however, would need to be lowered by a factor of ~ 4 in order to satisfy the GLUE upper limit. A better understanding of systematic effects in the GLUE experiment is needed before their results can be used to rule out models.

For comparison, the dotted curve in Fig. 5 shows the cosmic ray flux for protons originating from a uniform distribution of extragalactic sources with a constant comoving density. It is computed from

$$F_{EG}(E) = \int_0^\infty dE_p \int_0^{R_{max}} \frac{dr}{R_{max}} [1 + z(r)]^3 \\ \times F_p(E_p) \left| \frac{\partial P_p(r, E_p; E)}{\partial E} \right|, \quad (21)$$

where the unknown proton injection energy spectrum $F_p(E_p)$ is typically assumed to be a power law: $F_p(E_p) = \epsilon^{-1} A E_p^{-\beta}$. The shape of F_{EG} depends on the injection spectrum F_p , but for definiteness, we have assumed $\beta = 2.4$ and $A = 5.98 \times 10^{31}$ (and an upper energy cutoff of $E_p = 10^{23}$), which are found to be the best fit values

[24] to the existing cosmic ray data that have a total experimental exposure of $\epsilon \approx 8 \times 10^{16} \text{ m}^2 \text{ s sr}$. The GZK cutoff is clearly seen at $\sim 4 \times 10^{19} \text{ eV}$ in the dotted curve. The flux rises beyond $\sim 4 \times 10^{20} \text{ eV}$ because the photo-production of pions is a resonant process where the cross section peaks at $E_p \sim 2.3 \times 10^{20} \text{ eV}$ [1] and decreases at higher energies, allowing a larger fraction of protons to reach us.

The predictions for the UHECR spectrum change significantly when we incorporate the neutrino overdensity computed in Sec III. To make realistic estimates for our local universe, we consider five lines of sight towards five of the most massive nearby clusters: Virgo, Centaurus, Hydra, Perseus-Pisces, and Coma, where the highest overdensity of neutrinos are expected. The distance, mass, rough angular extent, and equatorial coordinates of each of the clusters are listed in Table 1 [50, 51]. The cluster masses are taken from <http://cfa-www.harvard.edu/huchra/clusters>, where they are estimated from galaxy velocities and the virial theorem. We caution that these values have large error bars. The mass of the nearest cluster Virgo [52–55], for example, has been estimated to be $1.5 - 6 \times 10^{14} M_\odot$ based on X-ray emission measurements by ROSAT [52], to $1.5 \times 10^{15} M_\odot$ based on the relativistic Tolman-Bondi method [53]. (The Tolman-Bondi model is based on analytic solutions to the Einstein field equations for spherically symmetric pressure free overdensities in a homogeneous universe [53, 56].)

Fig. 6 shows our predictions for the cosmic ray flux (in $(\text{eV m}^2 \text{ s sr})^{-1}$) towards these five lines of sight for four different neutrino masses. Along each line of sight, high energy neutrinos from extragalactic sources are assumed to traverse a uniform sea of background neutrinos plus an overdensity of background neutrinos centered at the location of the given cluster, where n_ν is computed from eq. (12) for the mass of the cluster. We also include in our calculation a local n_ν for the Local Group of mass $4 \times 10^{12} M_\odot$ [57]. Despite the smaller mass, the proximity of the Local Group to us leads to non-negligible contributions to the UHECR flux: about a factor ~ 2 for the $3 \times 0.6 \text{ eV}$ model, and up to a factor of ~ 10 at $E \gtrsim 10^{20} \text{ eV}$ for the 1.8 eV model. The difference is primarily due to the more efficient clustering of 1.8 eV neutrinos compared to 0.6 eV neutrinos in the Local Group.

Our main conclusion from Fig. 6 is that the flux of UHECRs in the Z-burst model should show significant anisotropy if $m_\nu \gtrsim 0.3 \text{ eV}$, with the largest flux coming from the Virgo cluster. For $m_\nu \lesssim 0.1 \text{ eV}$, on the other hand, neutrinos are too hot to cluster appreciably even around the largest clusters in the universe, and the UHECR flux in the Z-burst model is nearly isotropic. We choose to plot in Fig. 6 the flux per steradian because the angular extent of the clusters cannot be precisely defined, but one can easily use the approximate angular extents of the clusters listed in Table 1 to estimate the expected anisotropy in the signal.

V. CONCLUSION AND DISCUSSION

We have introduced and tested a method based on the collisionless Boltzmann equation to calculate the gravitational clustering of massive neutrinos in CDM halos for realistic cosmological models. This method is valid for currently favored models with $\Omega_{\text{cdm}} \gg \Omega_\nu$ in which the clustering of neutrinos is mostly determined by the existing CDM halos while the clustering of the CDM is little affected by the neutrinos. One can then obtain the neutrino phase space distribution by solving the collisionless Boltzmann equation in a background potential given by the universal profile of CDM halos from high resolution simulations. The resulting Boltzmann equation is linear in the neutrino density contrast and has tractable intergal solutions that require negligible computational time in comparison with N-body simulations. This method has enabled us to obtain specific predictions for the neutrino overdensity as a function of halo radius, halo mass, and neutrino mass for a wide range of parameters.

Our calculation shows that neutrinos with masses $\gtrsim 0.3 \text{ eV}$ can cluster appreciably in CDM potential wells with masses $\gtrsim 10^{13} M_\odot$. The predicted neutrino overdensity increases with both the neutrino mass and the halo mass, ranging from ~ 10 for 0.3 eV neutrinos in $\sim 10^{13} M_\odot$ halos to ~ 1500 for 1.8 eV neutrinos in $\sim 10^{15} M_\odot$. Specific predictions are plotted in Figs. 2 and 3. Neutrino clustering has a strong impact on the Z-burst model that has been proposed as a possible explanation for the UHECR events. The predicted UHECR spectrum shown in Figs. 5 and 6 depends sensitively on the neutrino mass and overdensity, showing distinct spectral features towards nearby galaxy clusters if $m_\nu \gtrsim 0.3 \text{ eV}$.

To illustrate the effects of neutrino mass and overdensity on the UHECR spectrum, we have chosen to normalize the flux in Figs. 5 and 6 with the same value (i.e. $F_{\nu_i}(E_{\nu_i}^{\text{res}}) = 1.7 \times 10^{-35} (\text{eV m}^2 \text{ s sr})^{-1}$ for each flavor for the three degenerate mass models and three times higher for the one massive species model) instead of adjusting it by fitting individual spectrum to existing data. We have nonetheless included current data from the AGASA [3] and HiRes [6] experiments in Figures 5 and 6 for comparison. More events are needed to discriminate the different models and the directional dependence. The large increase in flux towards Virgo is an interesting signature of the Z-burst model for upcoming experiments such as Auger [58] and OWL [59] that will provide an angular resolution of $\sim 1^\circ$. Experimental limits on the anisotropy would in turn imply small neutrino inhomogeneities in the Z-burst model and can be used to place upper bounds on the neutrino mass.

A useful constraint on the Z-burst model is provided by the Energetic Gamma Ray Experiment Telescope (EGRET) measurement of the GeV γ -ray background flux, which must not be exceeded by the high energy photons produced in the Z-burst models once they cascade down to the GeV energy range. The result depends on the assumed redshift evolution of the sources that pro-

TABLE I: Parameters of five nearby clusters

Name	Distance(Mpc)	Mass(M_{\odot})	Angular Radius($^{\circ}$)	RA(h min)	Dec($^{\circ}$ min)
Virgo	15	7.9×10^{14}	5	12 29.6	+11 49
Centaurus	43	1.3×10^{15}	1.5	12 46.1	-41 02
Hydra	53	4.6×10^{14}	2	10 34.5	-27 16
Perseus-Pisces	76	5.5×10^{15}	7	03 15.3	+41 20
Coma	99	1.7×10^{15}	2.5	12 57.4	+28 15

duce the incident high energy neutrinos, and on whether the sources themselves produce photons. The normalization of the neutrino flux cited in the previous paragraph rules out sources emitting a comparable flux in γ -rays because it leads to a conflict with the existing EGRET limits for the GeV γ -rays. For pure neutrino sources, calculations based on particle transport codes show that for neutrino masses of 0.1, 0.5, and 1 eV (ignoring neutrino clustering), the EGRET bound is met for $\alpha \lesssim -3$, $\lesssim 0$, and $\lesssim 3$, respectively, where the source number density evolves as $(1+z)^{\alpha}$ [24, 60]. When neutrino clustering is taken into account, our results from Fig. 2 show that the bound above for $m_{\nu} \lesssim 0.3$ eV should be unaffected since they do not cluster appreciably in the Local Group. For larger neutrinos masses, however, we expect a less stringent bound on the source evolution due to local neutrino clustering. To derive quantitative constraints would require detailed transport calculations.

The implications of the neutrino clustering results presented in this paper extend beyond the problem of the UHECR spectrum. For UHECR, upcoming experimental results may converge on a spectrum that is consistent with the GZK cutoff and would therefore not require models such as the Z-burst. It is also likely that the Z-burst model is not the correct explanation for the

UHECR events. However, the neutrino-anti-neutrino resonance scattering process remains one of few ways to detect the relic neutrinos, as first suggested in Ref. [18]. This paper has addressed neutrino clustering, a major uncertainty in all studies concerning relic neutrinos.

Acknowledgments

We thank Ed Bertschinger, Tom Weiler, Jon Arons, Bhuvnesh Jain, and Nick Sarbu for useful discussions. We also thank Dmitry Semikoz, John Beacom, and the referee for comments that have helped to improve the manuscript. C.-P. M. acknowledges support of an Alfred P. Sloan Foundation Fellowship, a Cottrell Scholars Award from the Research Corporation, and NASA grant NAG 5-12173. A portion of the work was carried out at the Aspen Center for Physics. This research has made use of the NASA/IPAC Extragalactic Database (NED) which is operated by the Jet Propulsion Laboratory, California Institute of Technology, under contract with the National Aeronautics and Space Administration and the Vizier catalogue access tool, CDS, Strasbourg, France.

-
- [1] K. Greisen, Phys. Rev. Lett. **16**,748 (1966); G.T. Zat'sepin and V.A. Kuz'min, J. Exp. Theor. Phys. Lett. **4**,78 (1966); R.J. Gould and G. Schreder, Phys. Rev. Lett. **16**,252 (1966).
 - [2] M. Nagano and A. A. Watson, Rev. of Mod. Phys. **72**, 689, (2000); A. V. Olinto, Phys. Rep. **333**, 329 (2000); P. Bhattacharjee and G. Sigl, Phys. Rep. **327**, 109 (2000); and references therein.
 - [3] M. Takeda *et al.* Phys. Rev. Lett. **81**,1163 (1998); updates at website <http://www-akeno.icrr.u-tokyo.ac.jp/AGASA>.
 - [4] D.J. Bird *et al.* [HIRES Collaboration], Phys. Rev. Lett. **71**,3401 (1993); Astrophys. J. **424**, 491 (1994); Astrophys. J. **441**,144 (1995).
 - [5] M.A. Lawrence, R.J. Reid and A.A. Watson, J.Phys. G **17**,733 (1991); M. Ave, J.A. Hinton, R.A. Vazquez, A.A. Watson and E. Zas, Phys. Rev. Lett. **85**,2244 (2000).
 - [6] The HiRes Collaboration, astro-ph/0208243; astro-ph/0208301.
 - [7] N.N. Efimov *et al.*, in *Proceedings of the Astrophysical Aspects of the Most Energetic Cosmic Rays* (World Scientific, Singapore, 1991).
 - [8] M.S. Longair, High Energy Astrophysics, Vol. 2, (Cambridge University Press, London, 1994); D. Fargion, R.V. Konoplich and A. Salis, Z. Phys. C **74**,571 (1997); D. Fargion and A. Salis, Phys. Uspekhi **41**(8), 823.
 - [9] D. Fargion and A. Salis, Nucl. Phys. Proc. Suppl. B **43**,269 (1995).
 - [10] J. Arons, astro-ph/0208444 and references therein.
 - [11] S. Fukuda *et al.* [Super-Kamiokande Collaboration], Phys. Rev. Lett. **86**, 5656 (2001) and references therein.
 - [12] M. Ambrosio *et al.* [MACRO Collaboration], Phys. Lett. B **517**,59 (2001).
 - [13] Q.R. Ahmad *et al.* [SNO Collaboration], Phys. Rev. Lett. **87**, 071301 (2001).
 - [14] J. Bonn *et al.*, Nucl. Phys. Proc. Suppl. **91**, 273 (2001).
 - [15] D. Fargion, B. Mele and A. Salis, Astrophys. J. **517**,725 (1999).
 - [16] T. Weiler, Astropart. Phys. **11**,303 (1999).
 - [17] G.M. Tanco, in *Physics and Astrophysics of Ultra-High-*

- Energy Cosmic Rays*, ed. M. Lemoine and G. Sigl (Springer), 155 (2001).
- [18] T. Weiler, Phys. Rev. Lett. **49**,234 (1982).
- [19] E. Roulet, Phys. Rev. D **47**,5247 (1993).
- [20] S. Yoshida, G. Sigl and S. Lee, Phys. Rev. Lett. **81**,5505 (1998).
- [21] G. Gelmini and A. Kusenko, Phys. Rev. Lett. **82**,5202 (1999); Phys. Rev. Lett. **84**,1378 (2000).
- [22] J.L. Crooks, J.O. Dunn and P.H. Frampton, Astrophys. J. **546**,L1 (2001).
- [23] Z. Fodor, S. D. Katz and A. Ringwald, Phys. Rev. Lett. **88**, 171101 (2002). [arXiv:hep-ph/0105064].
- [24] Z. Fodor, S.D. Katz and A. Ringwald, J. High Energy Phys. **0206**,46 (2002).
- [25] D. Fargion, hep-ph/0208093.
- [26] D. Fargion, M. Grossi, P.G.De Sanctis Lucentini, C. Di Troia, J.Phys.Soc.Jpn. Vol(70), Supplement B (2001).
- [27] J.F. Navarro, C.S. Frenk and S.D.M. White, Astrophys. J. **462**,563 (1996).
- [28] S. Tremaine and J.E. Gunn, Phys. Rev. Lett. **42**,407 (1979).
- [29] L. Kofman, A. Klypin, D. Pogosyan and J.P. Henry, Astrophys. J. **470**,102 (1996).
- [30] R. Brandenberger, N. Kaiser and N. Turok, Phys. Rev. D **36**,2242 (1987).
- [31] E. Bertschinger and P.N. Watts, Astrophys. J. **328**,23 (1988).
- [32] Ø. Elgarøy *et al.*, astro-ph/0204152.
- [33] J.F. Beacom and N.F. Bell, Phys. Rev. D **65**, 113009 (2002).
- [34] J.S. Bullock *et al.*, Mon. Not. R. Astron. Soc. **321**,559 (2001).
- [35] C.-P. Ma and J.N. Fry, Astrophys. J. **543**, 503 (2000).
- [36] C.-P. Ma and E. Bertschinger, Astrophys. J. **455**, 7 (1995).
- [37] S. Dodelson, E. Gates and A. Stebbins, Astrophys. J. **467**,10 (1996).
- [38] e.g., E.W. Kolb and M.S. Turner, *The Early Universe*, (Addison-Wesley Publishing Company,1990).
- [39] A. Kull, R.A. Trueman and H. Böhringer, Astrophys. J. **466**,L1 (1996).
- [40] V. Berezhinsky and A.A. Mikhailov, Phys. Lett. B **449**,237 (1999); G.A. Medina Tanco and A.A. Watson, Astropart. Phys. **12**,25 (1999); T. Weiler, hep-ph/0103023.
- [41] D.E. Groom *et al.* [Particle Data Group Collaboration], Eur. Phys. J. C **15**,1 (2000).
- [42] Z. Fodor and S.D. Katz, Phys. Rev. D **63**,023002 (2001).
- [43] M. Ave, J.A. Hinton, R.A. Vazquez, A.A. Watson and E. Zas, Phys. Rev. D **65**,063007 (2002).
- [44] K. Shinozaki *et al.* [AGASA Collaboration], in *Proc. 27th International Cosmic Ray Conference*, Hamburg, 2001.
- [45] R.J. Protheroe and P.L. Biermann, Astropart. Phys. **6**,45 (1996).
- [46] A. Venkatesan, M.C. Miller and A.V. Olinto, Astrophys. J. **484**,323 (1997).
- [47] E. Waxman, astro-ph/9804023; E. Waxman and J. Bahcall, Phys. Rev. D **59**, 023002 (1999); J. Bahcall and E. Waxman, Phys. Rev. D **64**, 023002 (2001).
- [48] G. Gelmini and G. Varieschi, hep-ph/0201273.
- [49] P.W. Gorham, K.M. Liewer and C.J. Naudet, astro-ph/9906504 Proc. of the 26th International Cosmic Ray Conference, Salt Lake City, Utah, (1999); P. Gorham, K.M. Liewer, C.J. Naudet, D.P. Saltzberg, and D.R. Williams, astro-ph/0102435.
- [50] F. Ochsenbein, P. Bauer and J. Marcout, Astron. Astrophys. Suppl. Ser. **143**,23 (2000).
- [51] NASA/IPAC Extragalactic Database.
- [52] H. Böhringer *et al.*, Nature **368**,828 (1994).
- [53] P. Fouqué, J.M. Solanes, T. Sanchis and C. Balkowski, Astron. and Astrophys. **375**,770 (2001).
- [54] R.B. Tully and E.J. Shaya, Astrophys. J. **281**,34 (1984); in *Evolution of Large Scale Structure*, ed. R.F.Stain and A.G.W. Cameron (ESO, Garching),333 (1998).
- [55] S. Schindler, B. Binggali and H. Böhringer, Astron. and Astrophys. **343**,420 (1999).
- [56] T. Ekholm *et al.*, Astron. and Astrophys. **351**, 827(1999).
- [57] I.M. Schmoldt and P. Saha, Astron. J. **115**,2231 (1998); D.M. Goldberg, Astrophys. J. **550**,87 (2001).
- [58] M. Kleifges *et al.* [Auger Collaboration], in *Proceedings of ICHEP 2000*, Osaka (World Scientific, 2000); Auger website <http://www.auger.org/>.
- [59] J.F. Krizmanic *et al.* [OWL/AirWatch Collaboration], in *Proceedings of the 26th International Cosmic Ray Conference*, Salt Lake City, 1999; OWL website <http://owl.gsfc.nasa.gov/intro.html>.
- [60] O.E. Kalashev, V.A. Kuzmin, D.V. Semikoz and G. Sigl, Phys. Rev. D **65**,103003 (2002).

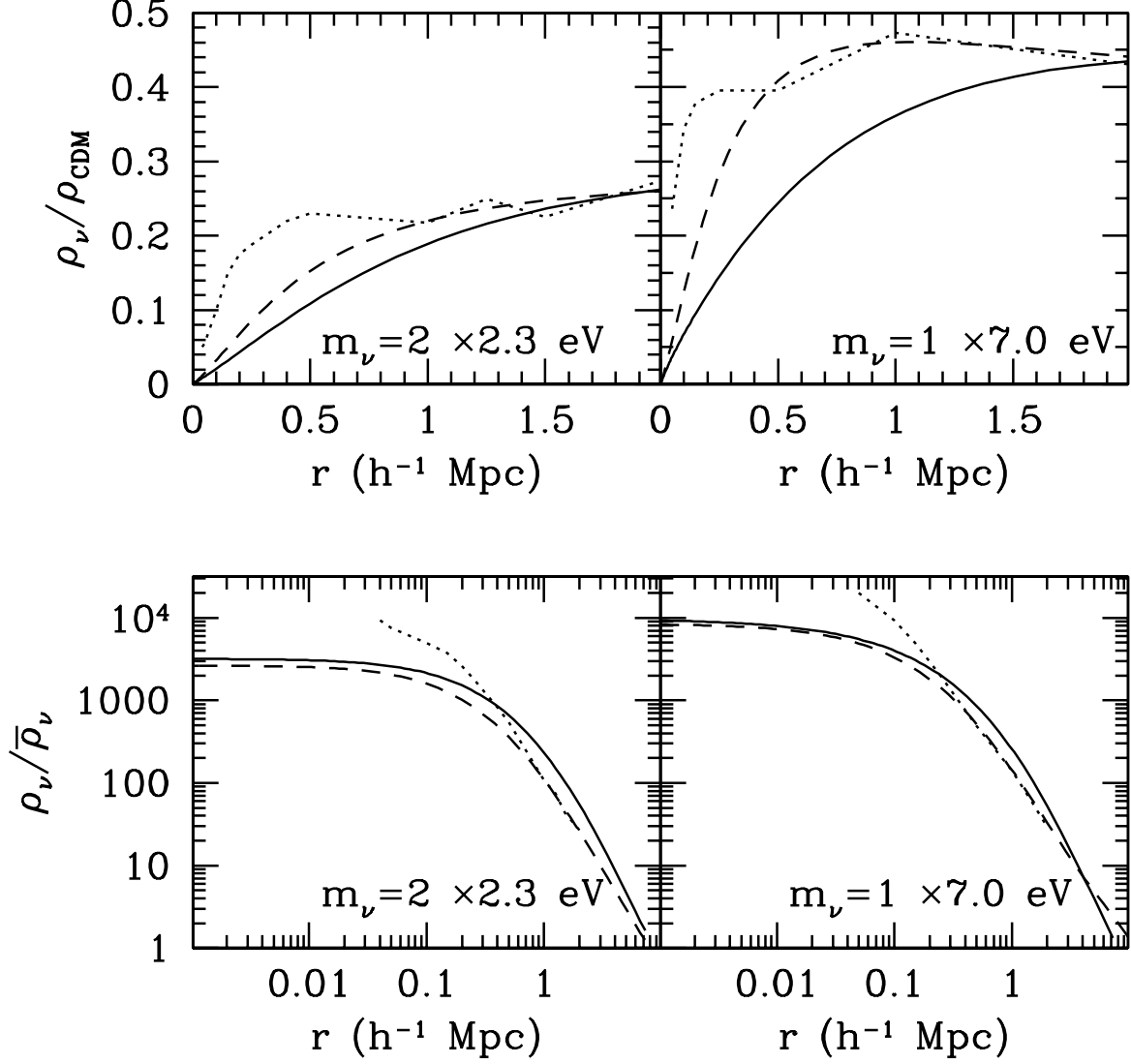


FIG. 1: Neutrino clustering calculated with our Boltzmann approach (dashed) vs. numerical simulations from [29] (dotted). The simulation resolution is $62.5 h^{-1}$ kpc. The upper panels show the ratio of the neutrino mass density ρ_ν to the CDM density ρ_{CDM} as a function of radius for two halos of $1.3 \times 10^{15} M_\odot$ in two cosmological models. The lower panels show $\rho_\nu/\bar{\rho}_\nu$ for the same models. The solid curves compare neutrino clustering around CDM halos with an NFW profile [27] to illustrate how neutrinos respond to different gravitational potentials.

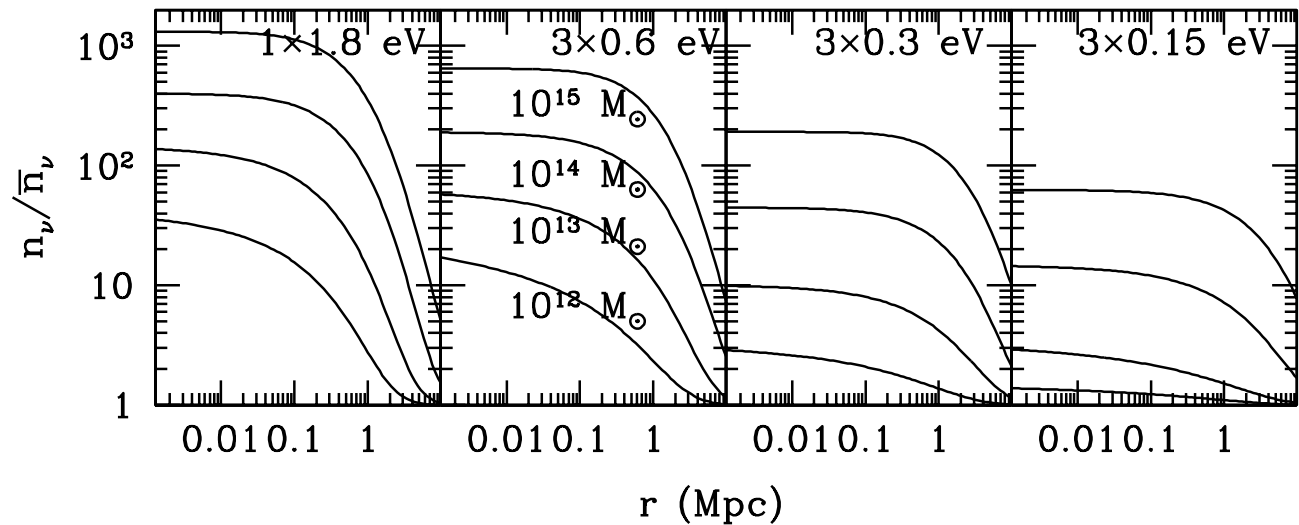


FIG. 2: Total neutrino number density $n_\nu(r)$ as a function of halo radius for different neutrino masses and halo masses at redshift 0. The curves are all normalized to $\bar{n}_\nu \approx 112 \text{ cm}^{-3}$ for ease of comparison. The four panels (from left to right) show how the clustering decreases as the neutrino mass is lowered, a result of increasing neutrino thermal velocity and more effective free streaming. Within each panel, the curves show how n_ν decreases as the halo mass is lowered from 10^{15} to $10^{12} M_\odot$, a result of shallower gravitational wells and smaller halo velocity dispersions compared with the neutrino thermal velocity. This figure shows that neutrinos with $m_\nu \gtrsim 0.15 \text{ eV}$ cluster appreciably in $M \gtrsim 10^{12} M_\odot$ halos.

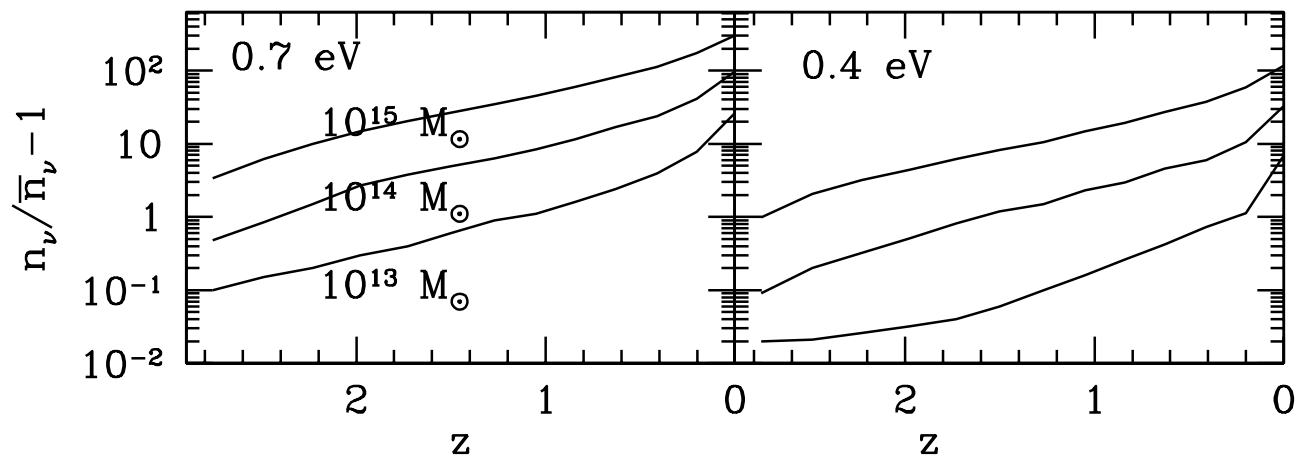


FIG. 3: Time evolution of the neutrino overdensity in the inner parts of the halos (where n_ν is independent of radius) for $m_\nu = 0.7$ (left) and 0.4 eV (right). In each panel, three halo masses 10^{15} , 10^{14} , and $10^{13} M_\odot$ are shown (top down). Neutrinos start to cluster significantly only at late times, with $\gtrsim 75\%$ of the clustering taking place between $z = 1$ and 0 .

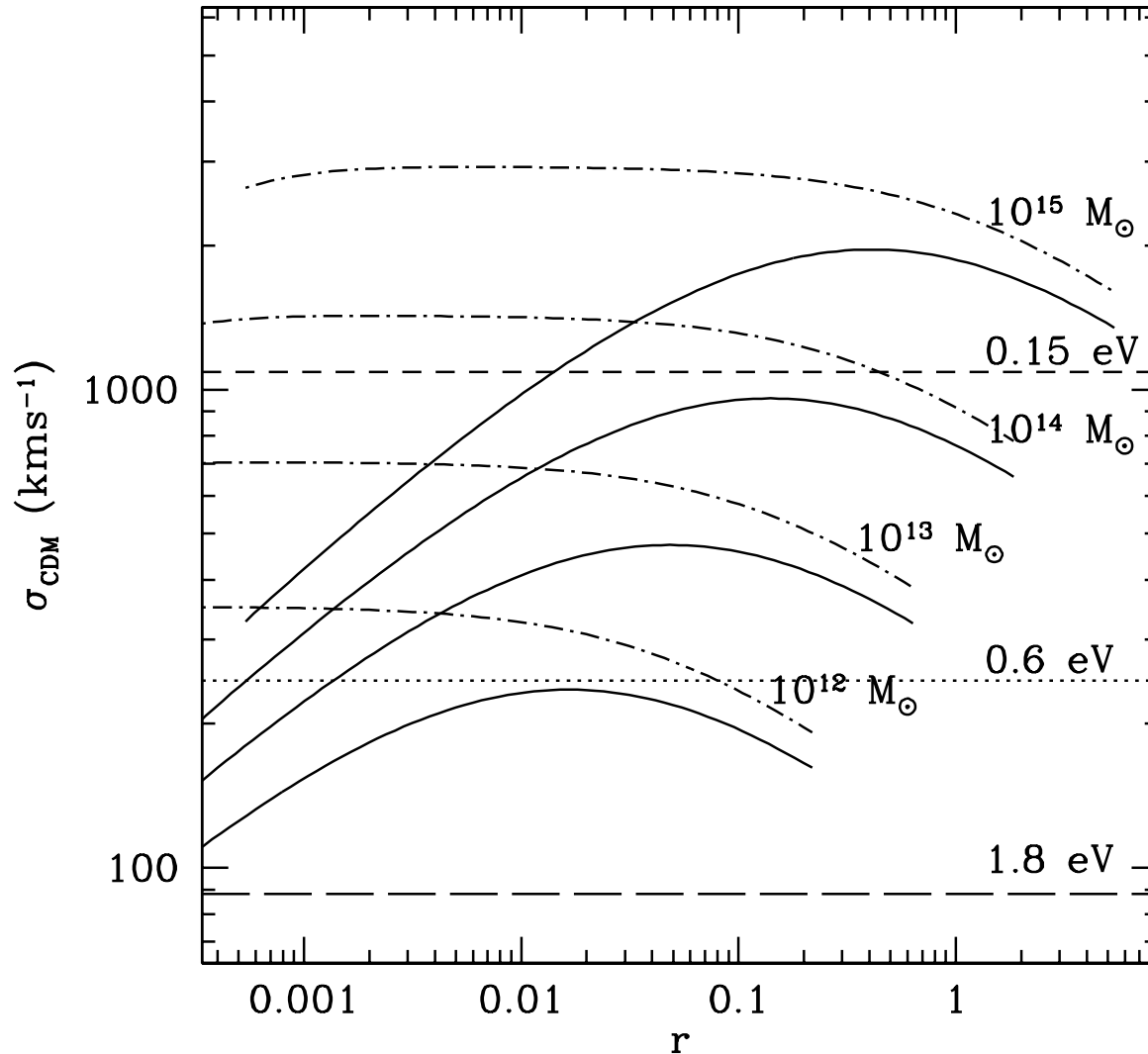


FIG. 4: Velocity dispersion of NFW halos of mass 10^{15} , 10^{14} , 10^{13} , and $10^{12} M_{\odot}$ (top down) as a function of halo radius. Two velocity orbits for the halo particles are shown for comparison: isotropic (solid) and $\beta \equiv 1 - v_t^2/v_r^2 = 0.5$ (dot-dashed). The horizontal lines indicate the present-day median thermal velocity for 0.15, 0.6, and 1.8 eV neutrinos. The values suggest that $m_{\nu} \gtrsim 0.15$ eV neutrinos are cold enough to cluster gravitationally, particularly in massive halos.

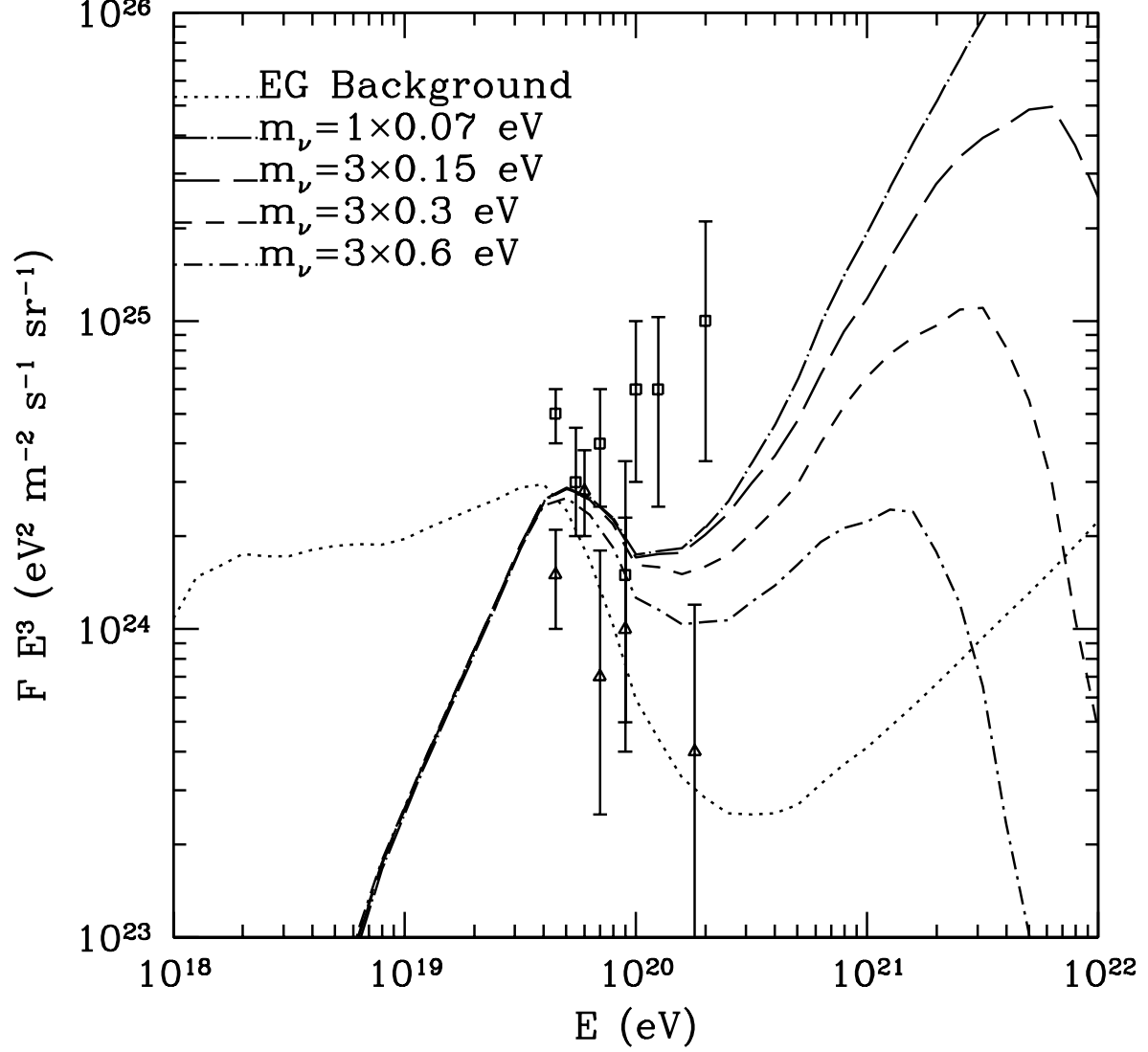


FIG. 5: Predictions for the cosmic ray flux produced in the Z-burst model when the relic neutrino density is assumed to be the big bang uniform background density without gravitational clustering. Three of the four models shown assume three degenerate masses, each with 0.6, 0.3, and 0.15 eV (from bottom up); the fourth model assumes a single massive species with 0.07 eV. The cosmic ray spectrum of protons originating from a uniform extragalactic background sources is shown for comparison (dotted). The GZK suppression in the flux is clearly seen at $E \gtrsim 4 \times 10^{19}$ eV in all spectra. The squares show the current 30 UHECR events from AGASA [3]; the triangles show the HiRes events [6].

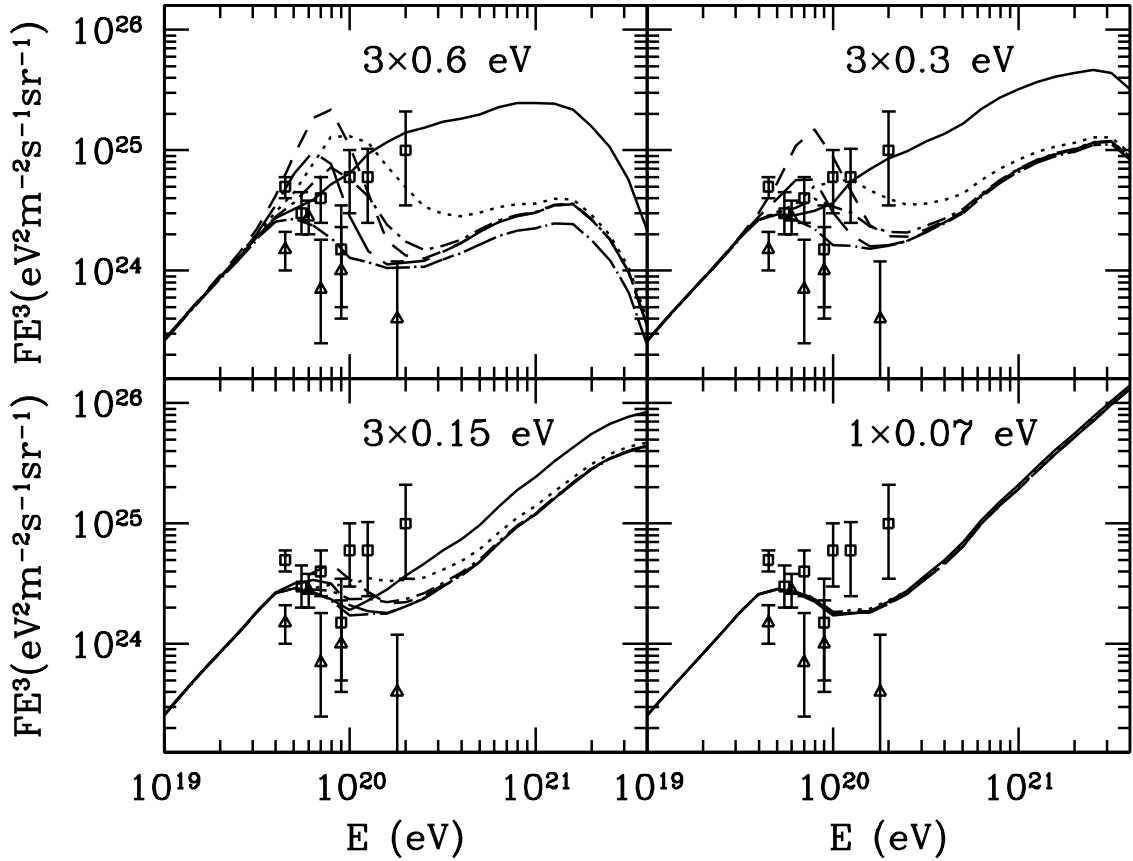


FIG. 6: Predictions for the cosmic ray flux produced in the Z-burst model using realistic neutrino overdensity computed in this paper. The four panels compare the UHECR spectrum for the same four neutrino mass models as Fig. 5. Within each panel, our predictions for the spectrum towards five of the most massive clusters in the local universe are shown: Virgo (solid), Centaurus (dotted), Hydra (dot short-dashed), Perseus-Pisces (short dashed), and Coma (long dashed). For comparison, the dot-long-dashed curve shows the spectrum when neutrino clustering is ignored (i.e. the same as in Fig. 5). For $m_\nu \gtrsim 0.3$ eV, we predict that the Z-burst model should produce distinct spectrum towards each line of sight. For $m_\nu \lesssim 0.1$ eV, neutrino clustering is insignificant and the spectrum is expected to be nearly isotropic as seen in the lower right panel. The data points are the same as in Fig. 5.